



Production of zeolitic materials in pilot scale based on coal ash for phosphate and potassium adsorption in order to obtain fertilizer

Beatriz Bonetti¹ · Etienne C. Waldow¹ · Giovanna Trapp¹ · Marta E. Hammercshmitt¹ · Suzana F. Ferrarini^{1,2} · Marçal J. R. Pires¹ · Sabrina T. Estevam³ · Thiago F. D. Aquino³

Received: 22 June 2020 / Accepted: 27 October 2020 / Published online: 5 November 2020
© Springer-Verlag GmbH Germany, part of Springer Nature 2020

Abstract

The use of different types of zeolites (X, Na-P1, and 4A) synthesized by different methods and scales were tested in this work to adsorb nutrients present in synthetic solutions and industrial effluents for later application as fertilizer. Modifications with calcium chloride were performed on the zeolite with the best performance to increase its adsorption capacity. The best performing zeolite was type X (ZXH) produced on a pilot scale by the hydrothermal process. Its adsorption capacity without modification was 149 mg P-PO₄/g zeolite and 349 mg K/g zeolite. With the change, there was a fourfold increase in these results, which were up to threefold higher than reported in the literature. The kinetic model that best characterized the adsorption process was the intraparticle diffusion model, and the equilibrium isotherm was that of Freundlich. The adsorption tests performed with industrial effluent showed high removal of the nutrients of interest (> 90% for PO₄³⁻ and > 95% for K⁺). The desorption tests with zeolites nutrient-loaded from synthetic solutions showed 13 to 24% PO₄³⁻ and 14 to 47% K⁺ release within 24 h, while for zeolite nutrient-loaded from effluent the release were 7 and 100% for PO₄³⁻ and K⁺, respectively. The results we obtained in this work indicated the potential use of zeolites in the treatment of effluent and its application as a fertilizer.

Keywords Zeolite · Pilot scale · Adsorption · Nutrients · Wastewater · Fertilizer

Introduction

In recent years, global coal power generation is estimated to have increased by around 3%, representing 40% of the world's energy generation. This increase has generated significant growth in the generation of ash, which, when stored or

disposed of incorrectly, causes damage to the environment (Gollakota et al. 2019). Thus, studies are aiming to reuse this residue, which is rich in silicon and aluminum, as a raw material in the development of new materials (Hemalatha and Ramaswamy 2017).

Zeolites are composed of silicon, aluminum, and oxygen and built by tetrahedrons (TO₄). The union of the tetrahedra forms typical secondary units and topology of the particle structure, resulting in micropores, channels, and cavities that generate specific properties of each type of zeolite (Rhodes 2010). Two methods are the most common among those used to convert coal ash into zeolites: the hydrothermal treatment, which consists of the hydrothermal reaction mechanism involving steps of dissolution, condensation, and crystallization of the material; and the fusion treatment, which consists of melting a mixture of ash and hydroxide, followed by the hydrothermal treatment (Izidoro 2013; Yoldi et al. 2019; Collins et al. 2020).

It is also worth mentioning the sparse studies on the influence of the scale increase of zeolite synthesis from ashes, which are essential for proving the viability of producing these materials on a commercial scale (Brassell et al. 2016). Zeolites

Responsible Editor: Tito Roberto Cadaval Jr

Supplementary Information The online version contains supplementary material available at <https://doi.org/10.1007/s11356-020-11447-y>.

✉ Beatriz Bonetti
beatriz.bonetti@acad.pucrs.br

¹ Materials Engineering and Technology, Pontifical Catholic University of Rio Grande do Sul, PUCRS, Porto Alegre, RS 90619-900, Brazil

² State University of Rio Grande do Sul–UERGS, São Francisco de Paula, RS, Brazil

³ Beneficent Association of the Santa Catarina Coal Industry, SATC, Criciúma, Brazil

are products of great commercial importance since their different structures allow their use in several applications, ranging from catalysts and adsorbents in the treatment of water and effluents to agricultural uses. For use as fertilizers, some studies have proposed the modification of zeolites with different compounds (Ca, Fe, La, among others) to increase the nutrient adsorption capacities (Bhardwaj et al. 2014; Ji et al. 2015; Hermassi et al. 2016, 2016; Mitrogiannis et al. 2017; Goscianska et al. 2018, 2018). Despite proven increases in nutrient adsorption, there is no assessment of the use of different types of zeolites for these applications.

The high content of nutrients in the aquatic environment is considered an aggravating factor to the environment since its excess causes eutrophication. Different technologies are presented in the literature on ways to treat wastewater for example, the use of clay for the treatment in effluent with dyes. (Ehsan et al. 2017; Kanwal et al. 2017; Nausheen et al. 2017; Kausar et al. 2018). Several authors have suggested the use of zeolites in the adsorption of nutrients such as phosphate and potassium present in different types of effluents (Wang and Peng 2010; Hamdi and Srasra 2012; Hermassi et al. 2016; Manto et al. 2017; Shi et al. 2017; Wan et al. 2017). Once loaded with nutrients, zeolites can be applied as a fertilizer and soil conditioner in agricultural systems (Bernardi 2008; Lateef et al. 2016; Harikishore Kumar Reddy et al. 2017; Guo et al. 2018).

Each plant has a different need for macronutrients for its development, such as N, P, and K, which despite being abundant in the soil, are difficult for plants to assimilate, mainly due to the way they are available (da Rocha Junior et al. 2017; Bruulsema 2018). According to the International Fertilizer Association, the fertilizer industry is committed to the sustainable use of all available sources of phosphorus. To this end, management practices for better recycling of this element and researches on new fertilizers produced from alternative sources, as is the case of this study, have been encouraged. It should also be noted that potassium-based fertilizers represent more than 90% of sales in countries such as Brazil and the USA.

The use of zeolites as fertilizers brings several associated benefits, such as increased nutrient loading capacity, cost reduction, control of the nutrient release rate, adaptability to soil conditions, and higher water retention. The use of the zeolite, synthesized from coal ashes, for obtaining fertilizers is extremely advantageous both from an economic and an environmental point of view since it makes it possible to add value to a waste that needs to find a suitable destination (Reddy et al. 2017).

In general, the studies reported in the literature focus on the use of natural zeolites or Na-P type zeolites, and there are no studies on type X zeolites. No studies are comparing the influence of synthesis processes on macronutrient adsorption. Although some studies use synthetic solutions of potassium phosphate salts, the simultaneous adsorption of the two compounds has not been discussed, since potassium, for example,

has been studied from its direct synthesis in the production of potassium zeolites (Flores et al. 2017; Liu et al. 2019).

The objective of this work is to test the adsorption of nutrients such as phosphate and potassium in different types of zeolites (Na-P1, A, and X), produced from different synthesis methods. Modification of the zeolite with greater adsorption capacity with calcium chloride (CaCl_2) was also carried out to further increase this capacity to develop a better quality product. The zeolite with the best performance was placed in contact with a real effluent to assess the adsorption capacity of nutrients and the influence of other contaminants present. Finally, it was evaluated the release of nutrients present in zeolites aiming at a possible application of the product as a fertilizer.

Methodology

Synthesis of zeolites

The zeolites used in this study were synthesized using two processes: (a) fusion followed by hydrothermal treatment and (b) integrated hydrothermal treatment. We also evaluated the bench scale and pilot scale synthesis. The two synthesis processes, at different scales, were studied to compare the purity and yield of the materials obtained and their performance in adsorption/desorption of nutrients. In both processes, fly ash was used, collected in the electrostatic precipitator of Unit 7 of the Jorge Lacerda Thermoelectric Plant (Capivari de Baixo- SC). In one of the synthesis tests by the fusion method, bottom ashes from that same unit were also used. We present the detailed procedures used in these syntheses in the Complementary Information file.

To compare the results of zeolites synthesized with high purity materials, we used commercial zeolites of the type Na-P1, 4A, and 13X (IQE, Spain), produced by the hydrothermal process from commercial inputs (usual reagents – no waste). Table 1 presents the synthesis conditions and the characteristics of the zeolites used in this work, which will be detailed below. The codes indicate the material (Z (zeolite)), the type (X, P, or 4A), and the method of synthesis used (F (fusion) and H (hydrothermal)).

Adsorption studies

Preliminary adsorption tests were carried out to evaluate the adsorption capacity of the synthesized zeolites and the process kinetics. The experimental conditions of these tests were based on procedures reported in the literature (Hermassi et al. 2016; Cheng et al. 2017; Goscianska et al. 2018). For that, solutions were prepared from potassium monobasic phosphate (KH_2PO_4), resulting in a concentration of 8.0 g $\text{PO}_4^{3-}/\text{L}$ and 3.2 g K/L.

Table 1 Identification, synthesis conditions, and basic characteristics of the zeolites used

| Zeolite | | Synthesis | | | | | |
|---------|-------|-----------|--------|---------------|------------|---------------|----|
| Type | Code | Process | | Scale | Ratio | Hydration (%) | |
| | | | | Si/Al** | | | |
| FAU | X | ZXC | Hydro | | Commercial | 1.0–1.5 | 27 |
| FAU | X | ZXF | Fusion | | Bench | 1.0–1.5 | 23 |
| FAU | X | ZXH | Hydro | Integrated II | Pilot | 1.0–1.5 | 24 |
| GIS | Na-P1 | ZPC | Hydro | | Commercial | 2.0–5.0 | 19 |
| GIS | Na-P1 | ZPF* | Fusion | | Bench | 2.0–5.0 | 8 |
| GIS | Na-P1 | ZPH. I | Hydro | Integrated I | Bench | 2.0–5.0 | 13 |
| GIS | Na-P1 | ZPH. II | Hydro | Integrated II | Bench | 2.0–5.0 | 18 |
| LTA | 4A | Z4AC | Hydro | | Commercial | 1 | 28 |
| LTA | 4A | Z4AH | Hydro | Integrated II | Pilot | 1 | 22 |

*Zeolite synthesized using heavy ashes

**Values determined according to Break (1975)

The tests were done in batches using Becker glass of 250 ml with the adsorbent (3.3 g) placed in contact with 200 ml of KH_2PO_4 solution (solid/liquid ratio 16.7 g L^{-1}). The mixture was kept under magnetic stirring (400 rpm) at room temperature ($23 \pm 1 \text{ }^\circ\text{C}$) and natural pH (6.21 ± 0.22) for 24 h. The 5 ml aliquots were removed at different times (5, 15, 30, 60, 180, 240, 300, 360, 420, 1380, and 1440 min), with the pH (Digimed DM-21) and electrical conductivity (SHOT Lab 960) being measured.

The phosphate and potassium adsorption capacities by zeolites were calculated from Eqs. 1 and 2, respectively.

$$\text{CAD}_P = \frac{\left[(\text{CI}_P - \text{CF}_P) \times \frac{\text{MMP}}{\text{MMPO}_4} \times 1000 \right] \times \frac{V}{1000}}{m_{\text{zeo}}} \quad (1)$$

where CAD_P is the phosphate adsorption capacity and expressed in mgP-PO_4 per gram of zeolite (wet basis); CI_P —initial phosphate concentration (g L^{-1}) in the solution; CF_P —final concentration of phosphate (g L^{-1}) in the solution; MMP—molar mass P (g mol^{-1}); MMPO_4 —molar mass PO_4 (g/mol); V volume solution (mL^{-1}); m_{zeo} mass of zeolite (g).

$$\text{CAD}_K = \frac{\left[(\text{CI}_K - \text{CF}_K) \times 1000 \right] \times \frac{V}{1000}}{m_{\text{zeo}}} \quad (2)$$

where CAD_K is phosphate adsorption capacity, expressed in mg K per gram of zeolite (wet basis); CI_K —initial K concentration (g L^{-1}) in the solution; CF_K —final concentration of K (g L^{-1}); V volume solution (mL^{-1}); m_{zeo} mass of zeolite (g).

Based on the preliminary tests' results, the other experiments were designed to assess equilibrium and kinetics in a wide range of concentrations and at different pHs. All other

experiments were carried out with the zeolites X (ZXF and ZXH) and Na-P1 (ZPH) that showed better performance in the preliminary test.

Adsorption kinetics

The results of the kinetics tests of the adsorption process, according to the procedure previously described, were obtained using the models of pseudo-first-order (Eq. 3) and pseudo-second-order (Eq. 4).

$$\log(q_e - q_t) = \log(q_e) - \frac{k_1}{2.303} t \quad (3)$$

$$\frac{t}{q_t} = \frac{1}{k_2 q_e^2} + \frac{1}{q_e} t \quad (4)$$

where: q_e (mg g^{-1}) is the amount adsorbed on the solid phase at equilibrium; q_t (mg g^{-1}) amount of material (phosphate) adsorbed at time t ; t (min) time; k_1 (min^{-1}) pseudo-first-order speed constant, and k_2 (g mg min^{-1}) is the pseudo-second-order model speed constant.

Different mechanisms occur during kinetics, in a process that involves transporting the adsorbate present in a liquid solution to a porous solid and intraparticle diffusion model described by Eq. 5.

$$q_t = k_i t^{1/2} + C \quad (5)$$

where: k_i ($\text{mg g}^{-1} \text{ min}^{-1/2}$) is the intraparticle diffusion rate constant, and C is the value of the intersection of the line with the q_t axis.

The models used were applied only to phosphate, since this is the element of main interest in this study. Potassium was monitored through the results obtained in the initial and final times in each adsorption test.

Adsorption in the function of pH

The adsorption test varying the pH of the solution from 4.0 to 9.0 was applied using solutions of NaOH (1 mol L⁻¹) and HCl (1 mol L⁻¹) to adjust the acidity/alkalinity following procedures reported in the literature (Jiang et al. 2013; Choi et al. 2016; Hermassi et al. 2016; Goscianska et al. 2018). These tests were performed with the zeolites X (ZXF and ZXH) and Na-P1 (ZPH) that showed better performance in the test at natural pH (6.21 ± 0.22).

The parameters adopted in these tests were the same as those described in sub-item “Adsorption studies”. At the beginning of the tests, the experimental conditions were monitored every 5 min, and after 60 min of contact, the monitoring was performed every hour, to maintain the pH stabilization of the solution in the desired range.

Adsorption isotherms

The evaluation of the phosphate and potassium adsorption equilibrium was carried out through isotherm tests following the experimental conditions reported in item “Adsorption studies” (natural pH, ambient T 23 ± 1 °C, S/L ratio 16.7 g g ml⁻¹, 400 rpm), with PO₄³⁻ concentrations varying from 1 to 40 g L⁻¹ and K⁺ from 0.4 to 16 g L⁻¹, and a total contact time of 5 h. The pH of the suspensions was measured at the beginning of the tests and corrected when necessary for the range of 6.0 ± 0.2 to maintain the conditions in which the adsorption of the material is favored, without the degradation of the zeolitic structure. The equilibrium capacities were determined using Eq. 6.

$$q_e = (C_o - C_e) \frac{V}{W} \tag{6}$$

where q_e is the equilibrium capacity, C_o (mg L⁻¹) and C_e (mg L⁻¹) represent the initial and equilibrium concentration of the analytes, respectively, v (L) is the volume of the solution, and w (g) is the zeolite mass.

The phosphate and potassium adsorption equilibria were evaluated according to the Langmuir (Eq. 7) and Freundlich (Eq. 8) isotherms.

$$\frac{C_e}{q_e} = \frac{1}{K_L q_m} + \frac{C_e}{q_m} \tag{7}$$

$$\log q_e = \log K_f + \left(\frac{1}{n}\right) \log C_e \tag{8}$$

where q_m (mg g⁻¹) is the maximum adsorption capacity, K_L (L mg⁻¹) is the Langmuir equilibrium constant, and K_F ((mg g⁻¹)/(mg L⁻¹)ⁿ) is the Freundlich equilibrium constant.

Desorption tests

The desorption test was performed with zeolites (0.5 g) loaded with different concentrations of phosphate and potassium in Na₂CO₃/NaHCO₃ (0.1 mol L⁻¹) buffer solution, with an pH of 10, at room temperature (23 ± 1 °C), with mechanical stirring (200 rpm) for 24 h (Onyango et al. 2007; Guaya et al. 2016; Hermassi et al. 2016). For type X samples, desorption was performed within 120 h, to follow the nutrient release process over a longer period. Desorption tests were also performed with zeolites after contact with effluent (item “Removal of nutrients present in effluents by zeolites”).

Modification of zeolitic material

To improve the adsorption capacity of nutrients, a modification of the zeolite with the best result (ZXH) was carried out, based on the adsorption tests performed (see item “Adsorption studies”). The modification tests were performed with CaCl₂ (0.5 M) solutions placed in contact with the sodium zeolite ZXH, successive cycles (five) of cation exchange being carried out until obtaining a high calcium loading. CaCl₂ was chosen because modified zeolite presented best nutrient adsorption capacities when compared to zeolites modified with Fe and La compounds (results not presented) and also is more advantageous in terms of reagents cost.

Removal of nutrients present in effluents by zeolites

With modified (ZXH.Ca) and unmodified (ZXH) zeolites, phosphate, and potassium adsorption and desorption tests were carried out in an industrial effluent with high concentrations of these nutrients. The methodologies followed for the tests were those described in items “Adsorption studies” and “Desorption tests” (S/L 16 ratio, 24 h, natural pH, 23 °C, 300 rpm). The industrial effluent was collected in a fertilizer industry located in Porto Alegre (RS-Brazil). The effluent comes from washing the company’s storage yards, which contain the fertilizer with varying concentrations of the nutrients of interest. The effluent is not treated being disposed directly into the water body.

Analytical methods

The concentrations of ions of interest (phosphate, potassium, and sodium) in the adsorption/desorption processes were analyzed by ion chromatography (IC) following the methodology developed by Philippi et al. (2007). The chemical composition of the adsorbents was analyzed by X-ray fluorescence (FRX) in a Shimadzu equipment, model EDX 7000, with a 3-kW tube and rhodium target.

The mineralogical composition of the zeolites before and after contact with the KH₂PO₄ solutions was also analyzed by

X-ray diffraction (DRX) using a Shimadzu equipment, model XRD-6100, with copper $K\alpha$ radiation, 40 kV power and 30 mA current. The ^{31}P analyses were performed on a nuclear magnetic resonance spectrometer (MAS NMR) with a BRUKER AVANCE HD III 400 MHz equipment, the peaks being identified with the aid of the DMFIT software (Ferrarini et al. 2016).

The total water content of the zeolites was determined by controlled heating, after saturation, according to the procedure mentioned by Abruzzi (2017).

The morphological analyses were performed using the scanning electron microscope (SEM), HITACHI model SU-70 coupled EDS system.

The variation in the composition of dissolved species as a function of pH was simulated using the chemical speciation software Visual MINTEQ. In these calculations, an aqueous solution containing only KH_2PO_4 (8 g/L in phosphate) was considered.

Results

Characterization of synthesized zeolites

The diffractograms of the synthesized materials and the commercial zeolites are shown in Fig. 1.

Type X zeolites, produced from fusion (ZXF) and hydrothermal (ZXH) methods at different scales, presented phases similar to commercial zeolite X, with characteristic 2θ angles (6° , 23.2° , 26.8° , and 31°). The sodalite phase is also present, but with low intensity. Its presence can be attributed to the excess of NaOH added or to the temperature maintained during the synthesis process, which also justifies the presence of amorphous phases (Aquino 2018). Another aspect related to the appearance of amorphous phases is the synthesis method since the precursor ash is converted directly into zeolite by the fusion method, for example, which causes undesirable impurities to remain in the material (Querol et al. 2002; Juan et al. 2007; Petrov and Michalev 2012; Izidoro 2013; Cardoso et al. 2015a; Brassell et al. 2016).

The chemical composition of the two synthesized type X zeolites (Table 2) was similar, being constituted by major elements Si and Al, expressed as the oxides of SiO_2 and Al_2O_3 . In addition to these, we highlight the presence of Na (Na_2O), which provides ion exchange through its mobilization with K^+ ions, and the presence of Ca and Fe, which assist in phosphate adsorption (Hermassi et al. 2016, 2016). P (P_2O_5) and K (K_2O) are also present in the structure, but in low concentrations ($< 1.5\%$). As expected, elements present in ash, such as Fe, Ca, Mg, Ti, and Mn (Aquino 2018), are present in greater quantity in zeolite synthesized by fusion (ZXF) compared to commercial zeolite (ZXC) and the one synthesized by the hydrothermal process (ZXH).

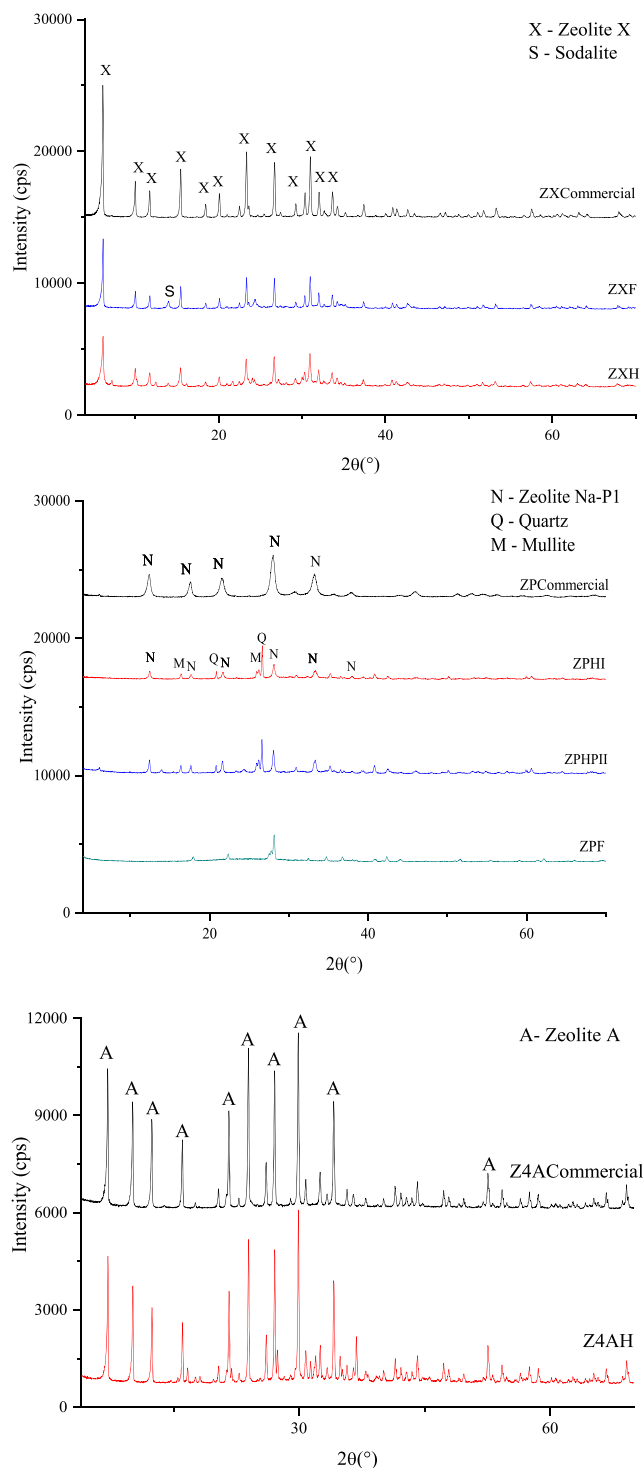


Fig. 1 Mineralogical characterization (XRD) of the commercial and synthesized zeolites used

To complement the characterization of the formed zeolitic material, scanning electron microscopy analyses were performed (Figure S1). The micrographs A (ZXF) and B (ZXH) refer to the formation of zeolites type X, with the classic configuration of an octahedral prism, proving the formation of the zeolitic material.

Table 2 Chemical composition of zeolites before contact

| Oxide | ZXH | ZXF | ZXC | ZPF | ZPH. I | ZPH. II | ZPC | Z4AH | Z4AC | ZXH. Ca* |
|--------------------------------|-------|-------|-------|-------|--------|---------|-------|-------|-------|----------|
| Content (%) oxides | | | | | | | | | | |
| SiO ₂ | 32.41 | 34.01 | 34.73 | 36.91 | 35.68 | 38.90 | 34.90 | 29.50 | 32.50 | 36.77 |
| Al ₂ O ₃ | 23.96 | 23.38 | 23.57 | 23.69 | 23.74 | 29.44 | 24.94 | 22.64 | 25.00 | 26.73 |
| Fe ₂ O ₃ | 0.08 | 2.82 | 0.07 | 4.05 | 2.92 | 3.84 | 0.07 | 0.06 | 0.05 | 0.30 |
| K ₂ O | 0.75 | 1.09 | 0.13 | 0.76 | 1.15 | 0.59 | 0.15 | 0.51 | 0.07 | 0.30 |
| CaO | 0.11 | 1.12 | 0.04 | 1.04 | 1.38 | 1.88 | 0.05 | 0.06 | 0.04 | 13.99 |
| TiO ₂ | 0.04 | 0.66 | 0.04 | 0.73 | 0.92 | 1.20 | 0.04 | 0.03 | 0.04 | 0.04 |
| MgO | 0.06 | 0.26 | 0.09 | 0.40 | 0.46 | 0.91 | 0.08 | 0.11 | 0.12 | 0.09 |
| P ₂ O ₅ | 0.03 | 0.04 | 0.03 | 0.04 | 0.05 | 0.05 | 0.03 | 0.03 | 0.03 | 0.18 |
| Na ₂ O | 17.57 | 1.39 | 15.02 | 12.96 | 13.48 | 9.25 | 19.23 | 19.26 | 18.98 | 3.08 |
| MnO | 0.03 | 0.39 | 0.00 | 0.52 | 0.50 | 0.68 | 0.03 | 0.02 | 0.08 | 0.02 |
| Total | 75.04 | 79.15 | 73.72 | 81.09 | 80.27 | 86.73 | 79.52 | 72.22 | 76.91 | 81.50 |
| PF | 24.96 | 20.85 | 26.28 | 19.73 | 20.85 | 13.27 | 20.48 | 27.79 | 23.09 | 18.50 |

*Type X zeolite modified with calcium chloride

Three zeolites type Na-P1 were synthesized on a bench scale, two produced from fly ash by the hydrothermal method (ZPH. I—Integrated Process I and ZPH. II—Integrated Process II), and one by fusion process with bottom ash (ZPF). It is noteworthy that the use of zeolite Na-P1 is the most recurrent in works presented in the literature (Xie et al. 2014, 2014; Hermassi et al. 2016; He et al. 2017; Goscianska et al. 2018, 2018), probably due to the greater ease of obtaining it both by hydrothermal methods and by fusion from coal ash (Querol et al. 2002; Cardoso et al. 2015a, 2015b).

The diffractograms obtained from the synthesized zeolites (see Fig. 1), when compared with that of the commercial zeolite, present angles 2 12.5°, 17.8°, 21.8°, 28°, and 33.2°, characteristic of the Na-P1 zeolite and also other phases like quartz and mullite. Izidoro (2013) comments that the presence of these phases is due to the synthesis process since they cannot be substantially dissolved, due to the amount of Fe present in the ash, which makes it difficult to release aluminosilicates, impairing the formation of the zeolite. In addition to these phases, the zeolite produced by the fusion process (ZPF) also presented magnetite, probably due to the use of bottom ashes in the synthesis process, which have a high iron content (> 7%) (Canpolat et al. 2004). Berggaut and Singer (1996) indicate that the presence of iron oxide does not favor the formation and growth of crystals, leading to partially formation of the zeolitic material. The major components present in this material were Si, Al, Na, and Fe (Table 2). P and K are also present in the structure, but in low concentrations (< 0.5%).

The mineralogical analysis of the ZPH. I sample is also presented, in addition to the characteristic phase of Na-P1, quartz and mullite phases, which are present in the ash and were not eliminated during the hydrothermal process (Cardoso et al. 2015b), were observed. The major components

present are Si, Al, and Na. Elements such as Fe, Ca, Mg, and K are also present in concentrations up to 7 times higher than those found in the commercial zeolite (ZPC), which probably hindered the formation of the zeolitic material. The zeolite produced by the Integrated Process II (ZPH. II) also had a characteristic DRX diffractogram of Na-P1 type zeolites with 2 12.5°, 17.8°, 21.8°, 28.0°, and 33.2°, besides quartz, mullite, and sodalite. The amount of sodium present in the synthesized zeolitic material is twice less than that present in the commercial zeolite, which compromises the formation of the zeolitic material (Querol et al. 2002). The three synthesized Na-P1 zeolites presented different micrographs (see Figure S1, C, D, and E). The ZPF (Image C) presented spheres typical of the precursor ash that indicate the partially formation of the zeolitic material. The images D and E referring to ZPH. I and ZPH. II, respectively, show the formation of the Na-P1 zeolite, with a similar structure to the reported in the literature (Querol et al. 2002; Cardoso et al. 2015a, b; Hermassi et al. 2016; Sharma et al. 2016).

Type 4A zeolite (Z4AH) was produced in a pilot scale synthesis process, and the X-ray diffractogram (Fig. 1) shows all angles 2 7°, 12.5°, 21.7°, 24°, 26.1°, 27.1°, 30°, 32.7°, and 34.1°, characteristic of this zeolite, which are also present in the diffractogram of the commercial Z4AC zeolite. There were no other phases or the presence of amorphous material in this sample, which suggests the formation of a product of higher purity (and crystallinity). These characteristics must be associated with the synthesis process that starts from ash extracts, basically containing Si and Al, and the addition of a supplemental source of Al (sodium aluminate). The chemical composition corroborates these results, with the presence mostly of SiO₂, Al₂O₃, and Na₂O. The SEM images (Figure S1F) referring to this zeolite show well-faceted cubes

with a regular surface, which are typical of this material (Cardoso et al. 2015b; Iqbal et al. 2019; Yang et al. 2019).

The total water content present in each synthesized material was determined in hydration tests since the formation and porosity are associated with the ability of molecular interaction on the internal and external surface (Pearce 1975). The zeolites with the highest moisture content (see Table 1) were type X (23 to 27%) and 4A (22%). The Na-P1 type zeolites had lower values (8 to 19%). The total water content is an indirect parameter, indicating the purity of the zeolite produced. This can be seen in the results obtained, since the commercial zeolites presented higher levels than the synthesized ones, which is expected, since the synthesized zeolites are produced from residues, having higher contaminations (Hu et al. 2017). Higher moisture content can be interesting to use as soil conditioners, which can be a vehicle for transferring chemical elements, nutrients, and other substances from the soil to the roots (Van Raji 2011).

Characterization of modified zeolite

Through XRD and FRX analyses, it was possible to confirm the modification of the zeolitic material without altering the main phases of the type X zeolite (ZXH). Figure 2 and Table 2 show the diffractogram and the chemical composition after the material has been modified, with the predominant phases of zeolite X being maintained at angles 2θ 6° , 23.2° , 26.8° , and 31° . The presence of calcite (CaCO_3) was also observed, being this phase due to the partial exchange of sodium ions present in the zeolite for calcium ions from the CaCl_2 solution (Hermassi et al. 2016). The incorporation of Ca can also be confirmed by the analysis of the FRX since, before the contact, the percentage of CaO was 0.11%, passing to 13.99%. Also, there was a significant decrease in the percentage of Na present in the sample (from 17.57 to 4.02%), which suggests

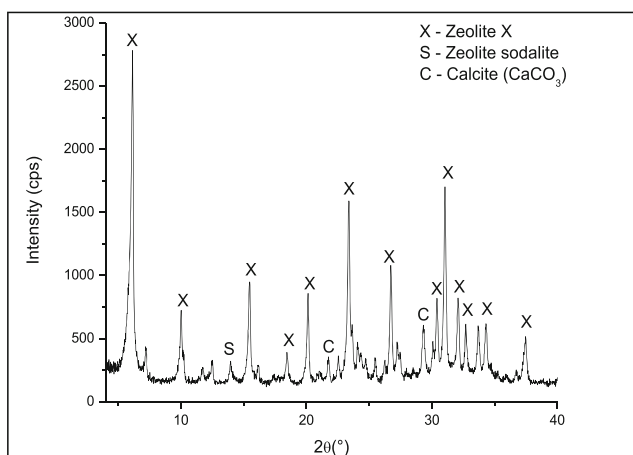


Fig. 2 Mineralogical characterization (DRX) and chemical composition of the modified zeolite ZXH. Ca

that the cation exchange process is the main mechanism of this modification process (Sandomierski et al. 2019).

Phosphate and potassium adsorption in zeolite

The adsorption capacities of phosphate and potassium ions for the six synthesized zeolitic materials and the modified zeolite (ZXH.Ca), as well as for three commercial zeolites, are shown in Fig. 3. In these tests, a solution with a concentration of PO_4^{3-} 8.0 g/L and K^+ 3.2 g/L (S/L ratio 16.7, 300 rpm, 25°C , natural pH ~ 6.2) was used. Figure S2 shows the adsorption capacities at different contact times, for a better evaluation of the different behaviors of the adsorbent materials studied.

The ZXF and ZXH zeolites showed the highest adsorption capacities, 55 and 47 mg $\text{P-PO}_4/\text{g}$ zeolite, respectively, and fast adsorption in the first 15 min of contact (70% of maximum capacity), followed by a longer period (20 to 200 min) until the adsorption equilibrium was reached (Figure S2). The Z4AH and ZPH. II adsorbents showed intermediate behavior with capacities of 27 and 35 mg $\text{P-PO}_4/\text{g}$ zeolite, respectively, and a longer time to reach equilibrium (350 min). The worst performances were observed for zeolite ZPH. I (17 mg $\text{P-PO}_4/\text{g}$ zeolite, equilibrium time 420 min) and ZPF (5 mg $\text{P-PO}_4/\text{g}$ zeolite, equilibrium time 420 min).

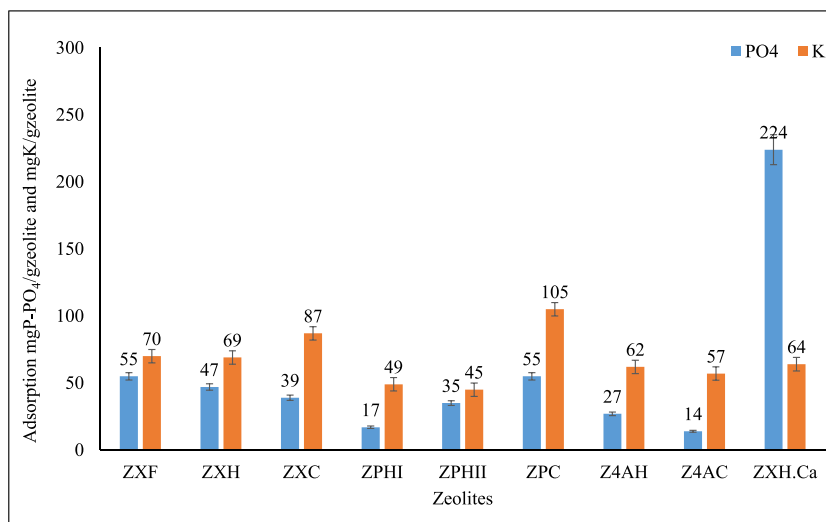
For commercial samples, it was observed that type X (ZXC) and 4A (Z4AC) showed lower adsorption performances (39 and 14 mg $\text{P-PO}_4/\text{g}$ zeolite, respectively) compared to the type X and 4A zeolites synthesized in this study, while the Na-P1 zeolite (ZPC) showed superior behavior (55 mg $\text{P-PO}_4/\text{g}$ zeolite). The increase in the contact time in up to 24 h did not significantly increase the phosphate adsorption in any of the adsorbents. This result indicates that shorter times can be used (maximum 5 h) to determine the maximum adsorption capacity, under these conditions.

For potassium, higher and differentiated adsorption capacities were observed when compared to phosphate adsorption capacities among the zeolites studied (Fig. 3). The commercial zeolites (ZPC, ZXC, and Z4AC) showed the highest adsorption capacities (105, 87, and 48 mg K/g, respectively) when compared to similar synthesized ones. The biggest differences are seen in the synthesized Na-P1 zeolites, which have less than half the capacity (45–48 mg K/g) of the commercial zeolite.

Regarding the FRX results obtained from the contact of zeolites, it is noted that before the ion exchange process (mobilization of Na^+ ions by K^+ ions), there is a predominance of the major elements of the zeolitic structure, that is, Si, Al, and Na, which correspond to more than 70% of the structure (Table 2). After contact with the KH_2PO_4 (8 g/L) solution, it is observed that Na is replaced in large part by K (Table 3).

The synthesized zeolites with the highest K percentage after contact were Z4AH and ZXH (10.12% and 9.42% K_2O , respectively). The zeolites ZXF, ZPH. I, and ZPH. II

Fig. 3 Maximum phosphate and potassium adsorption capacity in different types of zeolitic materials



also showed exchange rates, however, in lower quantities (< 8.15%). Commercial zeolites showed higher percentages than synthesized, being 15.46; 10.25, and 8.09% of K₂O, for the Z4AC, ZPC, and ZXC zeolites, respectively.

The possible mechanisms involved in adsorption and their relationship to the characteristics of each zeolite are complex (Hermassi et al. 2016). Zeolites can have basic sites, due to the oxygen atoms linked to Al, with which phosphate anions can interact, in addition to being retained by *extra-framework* cations (Ca, Na) and may also suffer interactions with Fe (Jha and Singh 2016).

The mechanisms that involve potassium absorption are mainly due to the cation exchange capacity of zeolitic materials (Flores et al. 2017). In their structure, formed by channels and cavities, zeolites have compensation cations and water molecules that are responsible for ion exchange, allowing the movement of cations to maintain their neutrality (Melo and Riella 2010). The main counterion present in the studied

zeolites is Na⁺, and its exchange for K⁺ depends on its concentration in solution and on the affinity with each type of zeolite (Liu et al. 2019).

Figure 4 shows the NMR for the analysis of the ZXH zeolitic material after being subjected to contact with the KH₂PO₄ (8 g/L) solution at natural pH (~ 6.2).

The RMN ³¹P spectrum of the zeolite exhibits a reference peak in the chemical environment -12.26 ppm. It is suggested from that, the formation of monodentate and bidentate phosphate complexes, since the presence of this signal occurred between - 21 and 0 ppm. The peak width, on the other hand, is characteristic of internal sphere surface phosphate complexes, linked to compounds present in the zeolite, such as Al and Fe, which indicates that there is no interposition of water molecules between the adsorbed molecules (Vilar et al. 2010; Zhan et al. 2017). Lopes (2017) comments that in regions close to - 50 ppm, phosphate species are bound to silicon present in the material structure. The author also comments that in positive

Table 3 Chemical composition of zeolites after contact with solution containing PO₄⁻ (8 g/L) and K⁺ (3.2 g/L).

| Oxide | ZXH | ZXF | ZXC | ZPF | ZPH. I | ZPH. II | ZPC | Z4AH | Z4AC | ZXH. Ca* |
|--------------------------------|-------|-------|-------|-------|--------|---------|-------|-------|-------|----------|
| SiO ₂ | 28.69 | 32.02 | 32.09 | 37.05 | 40.62 | 37.03 | 32.56 | 32.21 | 31.24 | 27.13 |
| Al ₂ O ₃ | 22.62 | 22.10 | 23.34 | 24.44 | 27.89 | 28.11 | 23.81 | 25.12 | 25.68 | 21.06 |
| Fe ₂ O ₃ | 0.09 | 1.83 | 0.04 | 1.97 | 2.60 | 2.65 | 0.06 | 0.06 | 0.07 | 0.06 |
| K ₂ O | 9.43 | 8.41 | 8.09 | 12.54 | 8.11 | 7.72 | 10.26 | 10.21 | 15.46 | 7.85 |
| CaO | 0.39 | 1.15 | 0.25 | 1.36 | 1.72 | 1.68 | 0.33 | 0.36 | 0.27 | 8.51 |
| TiO ₂ | 0.04 | 0.47 | 0.03 | 0.62 | 0.83 | 0.91 | 0.04 | 0.03 | 0.03 | 0.03 |
| MgO | 0.12 | 0.15 | 0.11 | 0.34 | 0.48 | 0.55 | 0.12 | 0.14 | 0.10 | 0.03 |
| P ₂ O ₅ | 14.33 | 9.51 | 5.44 | 5.41 | 3.88 | 7.61 | 10.13 | 3.16 | 3.13 | 24.03 |
| Na ₂ O | 5.40 | 5.33 | 6.52 | 2.54 | 1.29 | 1.09 | 6.74 | 7.98 | 3.76 | 0.90 |
| MnO | 0.01 | 0.29 | 0.02 | 0.13 | 0.46 | 0.53 | 0.02 | 0.01 | 0.01 | 0.00 |
| Total | 81.11 | 81.25 | 75.92 | 86.41 | 87.88 | 87.90 | 84.06 | 79.29 | 79.74 | 89.60 |
| PF | 18.89 | 18.75 | 24.08 | 13.59 | 12.12 | 12.10 | 15.94 | 20.71 | 20.26 | 10.40 |

*Type X zeolite modified with calcium chloride

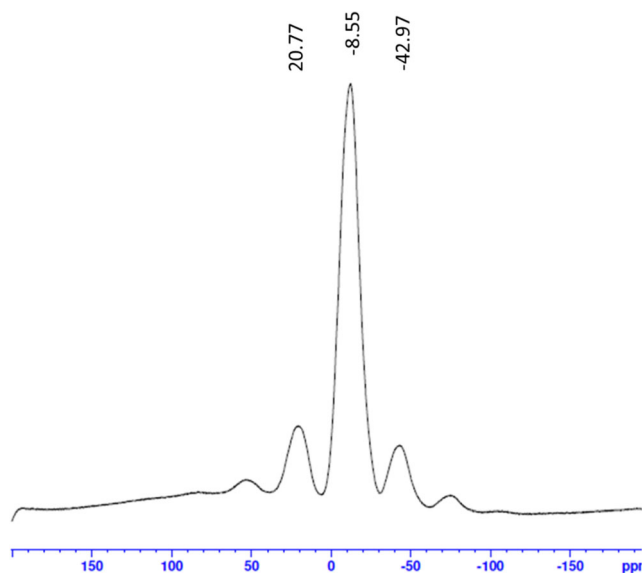


Fig. 4 ^{31}P NMR spectra of zeolite after 24 h contact with 8 g/L PO_4 solution

regions around 20 ppm, there is the presence of orthophosphate (PO_4) groups. Thus, the result achieved with the technique made it possible to confirm the adsorption of phosphate in the structure of the zeolitic material.

The modified zeolite (ZXHCa) showed a significant increase (~ 5 times) in the maximum adsorption capacity of P-PO_4 (224 mg $\text{P-PO}_4/\text{g}$ zeolite) when compared to ZXH without modification (47 mg $\text{P-PO}_4/\text{g}$ zeolite). Through the analysis of XRD after contact, the formation of the Brushite phase ($\text{CaHPO}_4 \cdot 2\text{H}_2\text{O}$) was confirmed (Figure S3), which is due to the formation of this mineral through the Ca that occupies the ion exchange sites of the zeolitic material (Hermassi et al. 2016). As expected, there was a great change in the chemical composition of the material (see Table 3) with a higher presence of Ca (8.51% CaO) compared to Na (0.90% Na_2O), in relation to zeolite without modification. The amount of P_2O_5 is also significantly higher (24.03%) than that observed in an unmodified zeolite (14.33% P_2O_5), confirming the higher incorporation of P in the structure. A large increase was also seen in the concentration of K (7.85% K_2O) in the modified zeolite after contact with the K_2HPO_4 (8 g/L) solution. These results suggest that Ca^+ can eventually be displaced by K^+ when occupying exchange sites. These data indicate that the zeolite ZXH. Ca has potential as a source not only of P but also of K in a fertilizer formulation.

Influence of the solution' pH on adsorption

The influence of pH on phosphate and potassium adsorption was studied for the synthesized zeolites that showed the best performance in preliminary tests (ZXF, ZXH, and ZPH. I) and modified zeolite (ZXH. Ca). These tests were carried out under the same conditions as the adsorption tests, with the pH

being varied from 4.0 to 9.0 and maintained throughout the contact time (5 h). The results obtained for phosphate and potassium adsorptions are shown in Table 4.

It is noted that in an acid medium, there was a considerable increase in the phosphate adsorption capacity, reaching maximum values at pH 5 for zeolites type X (86, 115, and 288 mg $\text{P-PO}_4/\text{g}$ zeolite) and at pH 4 for Na-P1 zeolite (63 mg $\text{P-PO}_4/\text{g}$ zeolite). For the four materials at basic pH, there was a decrease in the adsorption capacity, with pH 9 being the worst performing band: 20, 12, 7, and 120 mg $\text{P-PO}_4/\text{g}$ zeolite for ZXF, ZXH, ZPH. I, and ZXH. Ca, respectively.

In an acidic environment, a similar behavior was observed in potassium adsorption (Table 4), with the highest adsorption capacities at pH 5 for the zeolites: ZXH (114 mg K/g), ZXF (130 mg K/g), ZPH. I (54 mg K/g), and ZXH. Ca (288 mg K/g).

Due to the variation in the adsorption capacity according to the pH, after the contact tests, the XRD analysis of the zeolitic material was performed (Fig. 5). At low pHs, there was a degradation of the zeolitic material ZXF and ZXH, indicating that under these conditions, the material structure is compromised. The Na-P1 zeolite (ZPH. I) maintained its structure better, despite having considerably reduced the intensity of the peaks characteristic of this type of material. It should be noted that the highest phosphate and potassium adsorption capacities occurred at pH 4–5 where the zeolite structures already show degradation with the probable release of aluminum species. These structures can play an essential role in adsorption, especially for phosphate. On the other hand, the additional increase in acidity (pH 3–4) of the contact solution reduces the amount of phosphate and potassium retained in the adsorbent, indicating that the adsorption mechanism is complex. Despite the higher values of phosphorus and potassium adsorption occurring in acidic conditions, the importance of maintaining the zeolitic structure to obtain a slower desorption process is emphasized, which can be beneficial for the use of materials as fertilizers.

Table 4 Capacity of adsorbents after contact with solution containing PO_4^- (8 g/L) and K^+ (3.2 g/L) at different pHs

| pH | ZXF mg-P- PO_4/g zeolite | ZXH mg-P- PO_4/g zeolite | ZPH. I mg-P- PO_4/g zeolite | ZXH. Ca mg-P- PO_4/g zeolite | ZXF mg-K/g zeolite | ZXH mg-K/g zeolite | ZPH. I mg-K/g zeolite | ZXH. Ca mg-K/g zeolite |
|----|---|---|--|---|-----------------------|-----------------------|--------------------------|---------------------------|
| 9 | 20 | 12 | 7 | 120 | n.m | n.m | n.m | n.m |
| 8 | 18 | 25 | 19 | 167 | n.m | n.m | n.m | n.m |
| 7 | 29 | 47 | 20 | 196 | n.m | n.m | n.m | n.m |
| 6 | 55 | 48 | 19 | 224 | 86 | 69 | 49 | 196 |
| 5 | 86 | 114 | 47 | 288 | 130 | 114 | 54 | 288 |
| 4 | 65 | 104 | 63 | 270 | 55 | 51 | 36 | 270 |
| 3 | n.m* | n.m | 61 | n.m | n.m | n.m | 23 | n.m |

*n.m., Unmeasured

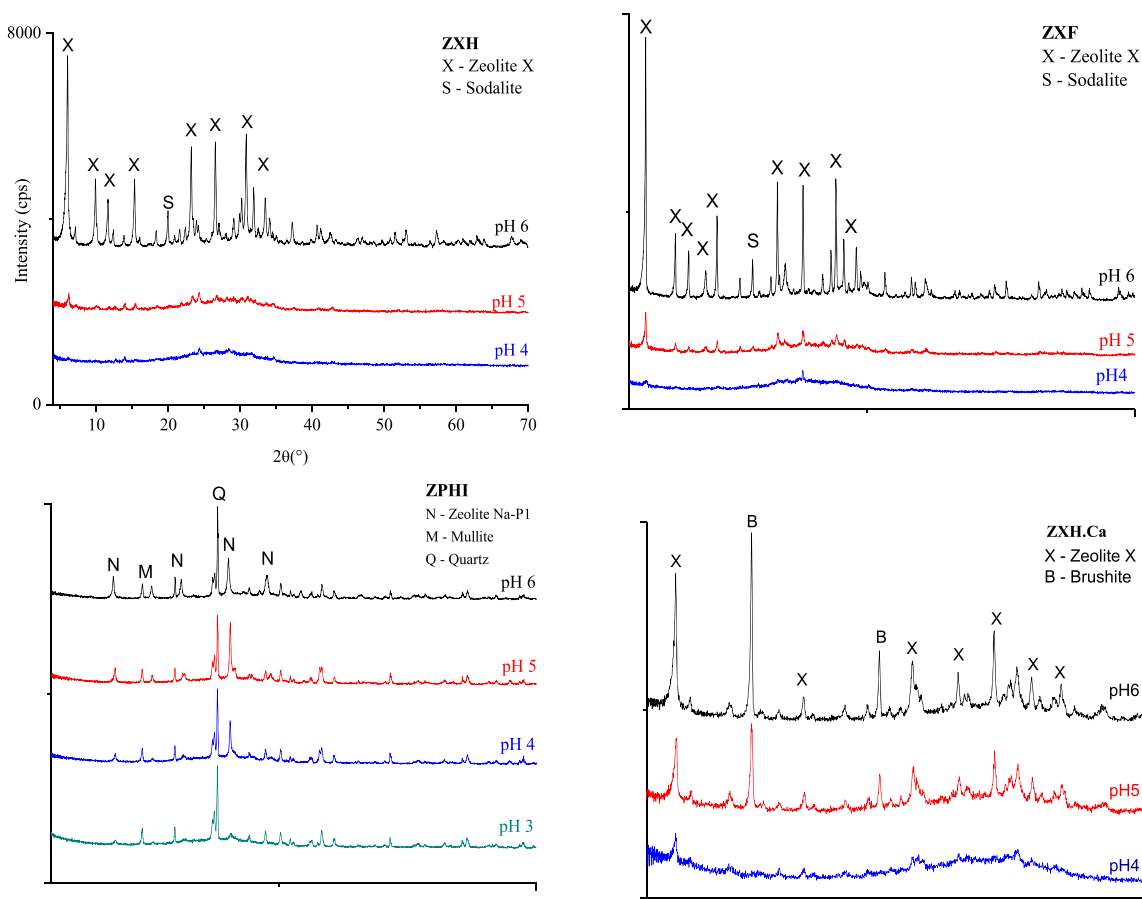


Fig. 5 Mineralogical characterization of zeolites ZXH, ZXF, ZPH, I, and ZXH. Ca after contact with 8 g/L solutions of P-PO4 at different pHs

Figure 6 presents the data from the simulation of phosphate and potassium speciation in an aqueous solution of K_2HPO_4 (8 g/L) as a function of pH using Minteq software. According to the pH variation (Fig. 6a), there is a variation in the phosphate species present, at pHs between 3 and 6, the predominant species is $H_2PO_4^-$ and, since the adsorbent surface is positively charged by protonation, there is a higher interaction between the zeolitic material with this species, thus increasing

the adsorption capacity (Goscianska et al. 2018). In basic zones, $pH > 7$, the effects of electrostatic interaction and ion exchange weaken, since deprotonation occurs on the surface of the adsorbent, thereby decreasing its interaction with the predominant phosphate species in an alkaline medium (HPO_4^{2-}).

The presence of potassium changes the balance of phosphate species (Fig. 6b), with the formation of KH_2PO_4 at pH

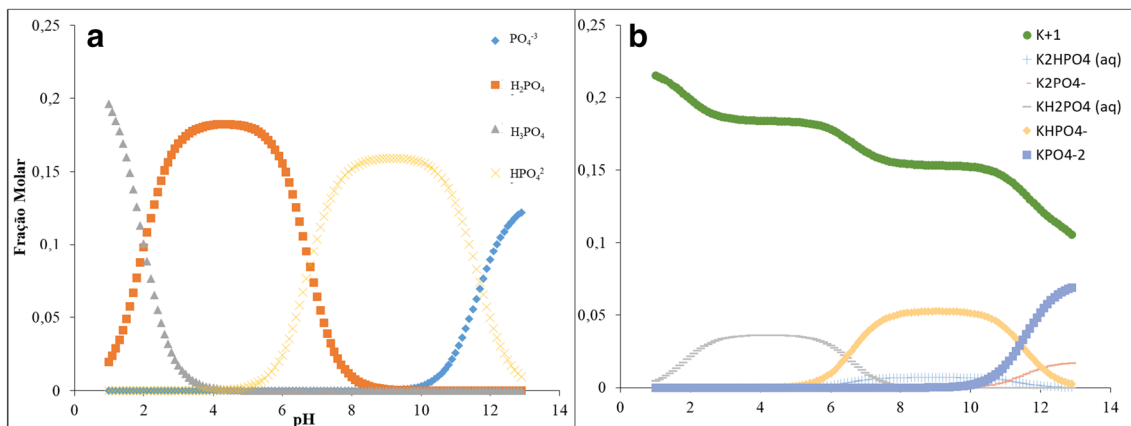


Fig. 6 Chemical speciation in aqueous KH_2PO_4 solution as a function of pH obtained by the Minteq application: a phosphate species and b potassium and phosphate species

between 2 and 6 and KHPO_4^- at $\text{pH} > 6$, with the consequent decrease in free K^+ in solution with increasing pH. This behavior may explain the lower potassium adsorption (5 times less) in alkaline pHs.

Adsorption isotherms

The results obtained in the adsorption tests with different initial phosphate concentrations (1 to 20 g PO_4/L) by the zeolites ZXH, ZXF, and ZPH. I and by the modified zeolite ZXC. Ca were applied in the models of the Langmuir and Freundlich isotherms. The Langmuir model describes an adsorption process that leads to the formation of a monomolecular layer on the surface of the adsorbent, the principal adsorption mechanism occurring on the surface of the zeolite. Freundlich's model is used to describe adsorption processes in heterogeneous systems. The results obtained in this work are shown in Table 5.

In the Langmuir model, the correlation coefficient R^2 showed ranges that varied from 0.9179 to 0.9885, which are smaller than the coefficients obtained by the Freundlich model. The highest KL value (0.008 L/mg) was obtained for the ZXC. Ca sample, which means that this material exhibits the highest selectivity in relation to phosphate, which can be proven with the maximum adsorption value of this zeolite (625 mg P- PO_4/g).

The behavior of the studied zeolites was better described by the Freundlich isotherm since the R^2 for the four adsorbents was higher than 0.98. It should be noted that the constant $1/n$ indicates the heterogeneity factor, which is related to the affinity of the adsorbent to the adsorbate. The affinity is higher when this factor tends to zero, which suggests that the surface adsorption conditions were favorable. Other studies have also indicated the Freundlich model as the most adequate to describe the phosphate adsorption in zeolites without modifications (Pengthamkeerati et al. 2008; Hermassi et al. 2016).

In addition, at low concentrations (30 to 100 mg P- PO_4/L), the phosphate adsorption capacity in zeolites increased significantly with the increase in the equilibrium concentration, indicating a high affinity of the phosphate ion binding sites. In higher concentrations, the adsorption capacities are less intense,

which is the result of the higher occupation of the active sites. Onyango et al. (2007) comment that this type of behavior is interesting since high adsorption in low equilibrium concentration will allow the treatment of a large volume of water before the replacement or regeneration of the adsorbents.

It is important to highlight that with the isotherm tests, it was possible to evaluate the maximum adsorption capacity of P- PO_4 for the zeolites without modification ZXH, ZXF, and ZPH. I, which were 190, 159, and 74 mg P- PO_4/g zeolite, respectively. These results, when compared with those reported in the literature using unmodified zeolites (Table 6), are promising for the application of the zeolites synthesized in this work. For modified zeolite (ZXC. Ca), it was possible to verify that the result obtained in this study (625 mgP- PO_4/g) was three times higher than that reported in literature (Wu et al. 2008; Zhang et al. 2012; Xie et al. 2014; Hermassi et al. 2016; Goscianska et al. 2018).

Adsorption kinetics

The curves obtained by the pseudo-first-order and pseudo-second-order models referring to zeolite ZXH are shown in Fig. 7a, b. It was found that the pseudo-second order model presented a better fit to the experimental data. The values of R^2 and of fit coefficients corresponding to each model are shown inside the figures.

Different mechanisms occur during kinetics, and several models can be used to provide an understanding of the process that involves transporting the adsorbate present in a liquid solution to a solid surface. One of the models that explain this mechanism is that of intraparticle diffusion (Chmielewska et al. 2013). The results for this model are shown in Table 7, and the graphical representation of the ZXH zeolite is in Fig. 7c.

A two-stage behavior is consistently observed with the amount of P captured, as mentioned above, having a rapid increase in the first 15 min, and then the sorption rate decreases dramatically. For all sorbents, the coefficients calculated for the diffusion of the pore (k_d, p) are up to 20 times lower than those of the film diffusion (k_d, f), indicating that the diffusion through the micropores within the zeolites is the limiting process.

Table 5 Isothermal parameters of phosphate sorption in different zeolitic materials

| Zeolite | Langmuir | | | Freundlich | | |
|---------|---------------------------------|---------------------------------|--------|--|--------|--------|
| | q_m (mg g^{-1}) | K_L (L mg^{-1}) | R^2 | K_f ($(\text{mg g}^{-1})/(\text{mgL})^{1/n}$) | $1/n$ | R^2 |
| ZXH | 190 | 0.002 | 0.9538 | 0.002 | 0.8804 | 0.9807 |
| ZXF | 159 | 0.001 | 0.9179 | 0.014 | 0.8840 | 0.9817 |
| ZPH. I | 74 | 0.001 | 0.9885 | 0.005 | 0.9487 | 0.9917 |
| ZXH. Ca | 625 | 0.008 | 0.9707 | 0.944 | 1.6379 | 0.9766 |

Table 6 Comparison of the maximum adsorption capacities obtained in this study with data from the literature

| Type of zeolite | Method | Code | Maximum adsorption capacity mgP-PO ₄ /g | | Concentration of the mgPO ₄ /L solution | pH | Reference |
|-----------------|--------------|---------|--|-------------------|--|-------|--------------------------|
| | | | Unmodified zeolites | Modified zeolites | | | |
| X | Hydrothermal | ZXH | 190.0 | 625.0 | 20000 | 6.50 | This study |
| X | Fusion | ZXF | 159.0 | n.m* | " | 6,50 | This study |
| NaP1 | " | ZPH | 74.0 | n.m | " | 6.50 | This study |
| NaP1 | " | NaP1-Fa | 57 | 203 | 16000 | 8,00 | Hermassi et al. (2016) |
| NaP1 | " | NA-P1 | 11.4 | 58.2 | 200 | 5.30 | Goscianska et al. (2018) |
| NaP1 | " | ZFA | 6.1 | 71.9 | 1530 | 10.00 | Xie et al. (2014) |
| NaP1 | " | ZHZ | n.m | 7.4 | 500 | 7.00 | Fan et al. (2017) |
| Natural zeolite | " | Zeo N | 0.6 | 3.4 | 6130 | 8.00 | Guaya et al. (2015) |

*n.m Uninformed

The multilinearity present in the intraparticle diffusion model is characterized by three main stages. The first stage, corresponding the film diffusion, is attributed to the solid surface layer of the zeolitic material. The adsorption kinetic rate is fast since the interaction between the adsorbate and the adsorbent is direct. The second stage is characterized by the diffusion on particles pores, which occurs slowly because the external surface of the adsorbent has reached saturation. The phosphate ions adsorbed into the solid fill the internal pores of the material, increasing the resistance to intraparticle diffusion. The final equilibrium phase begins when the speed of diffusion decreases due to the low concentration of solute in the solution and the smaller amount of active adsorption sites available (Onyango et al. 2007; He et al. 2016; Manto et al. 2017).

Figure S4 shows the ratios between the maximum adsorption capacity and those obtained in 5, 15, and 60 min of contact. It is observed that the ZXH, ZXF, and ZPH. I samples reach 50% of their total adsorption capacity in up to 5 min, with ratios close to 80% in the first 60 min, followed by a slower process until reaching equilibrium in 300 min of contact. The same conditions are observed with the modified zeolite (ZXC.Ca) since its maximum capacity is reached within 60 min of contact.

According to He et al. (2016), the rapid adsorption caused in the first stage (within 60 min) is probably due to the active sites available on the surface of the material, becoming less efficient with their gradual occupation during the adsorption process. Besides, Onyango et al. (2007) comment that the affinity of phosphate for active sites is strong so that the process of mass transfer within the particles is a limiting factor in the rate of the adsorption process.

Phosphate and potassium desorption

For the desorption tests, a Na₂CO₃/NaHCO₃ (0.1 mol L⁻¹, pH 10) buffer solution was used because the phosphate ions are displaced by the bicarbonate ions, favoring the release of the adsorbent (Hermassi et al. 2016). Figure 8 shows the

percentages of phosphate and potassium desorption obtained for each type of zeolitic material.

Despite being different materials, in the first 24 h of testing, the range of phosphate desorption between zeolites of type X and Na-P1 was similar, varying from 13 to 25%, indicating that the use of these types of materials allows more slow release of this nutrient. By monitoring the ZXH zeolite within 120 h, it was possible to confirm this type of release since the total release at this time did not reach 50% of the initial capacity.

The potassium desorption mechanism is associated with the influence of the buffer solution through the exchange mechanism between Na and K, as mentioned in item “Phosphate and potassium adsorption in zeolite”. Table 8 shows the variation in the chemical composition of loaded and desorbed zeolites, indicating that sodium has been incorporated into the zeolitic material at the same time that potassium has been released.

When compared to phosphate releases, the percentages of potassium release were higher (14 to 50%), having been subjected to the same test conditions. As with phosphate, potassium release analysis was also performed within 120 h. Contrary to the behavior evaluated for phosphate, for zeolite ZXH, there was an increase in the release of potassium in the first 48 h (44%), decreasing to 8% in 120 h, indicating that the exchange of potassium with sodium was saturated.

It is also important to note that the chemical composition before and after the desorption analyses, except for the exchange of K and Na ions, remained similar for all types of zeolitic materials, suggesting that the zeolite structures were maintained, which corroborates with the use of these materials as fertilizer.

Adsorption of nutrients present in the effluent

The pH, conductivity, and chemical compositions of the effluent before and after contact with zeolite ZXH. Ca are

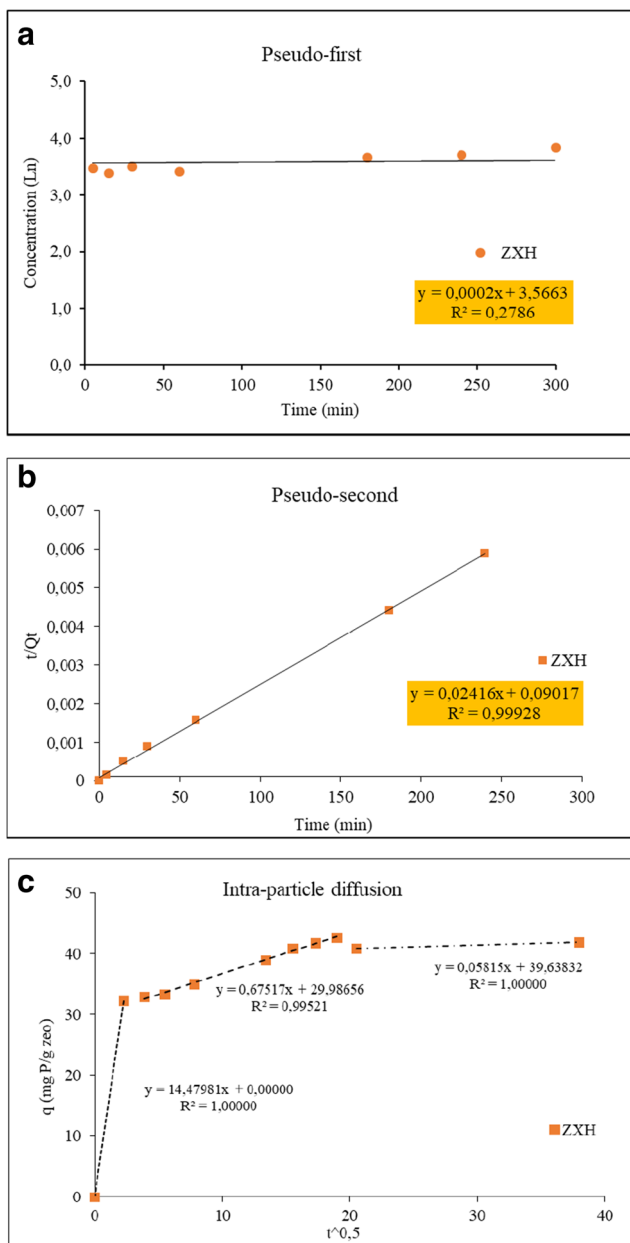


Fig. 7 Kinetic models of pseudo-first-order, pseudo-second-order, and intraparticle model for phosphate adsorption in ZXH zeolite (16S/L, pH 6, ambient T, conc. 8 g/LPO₄)

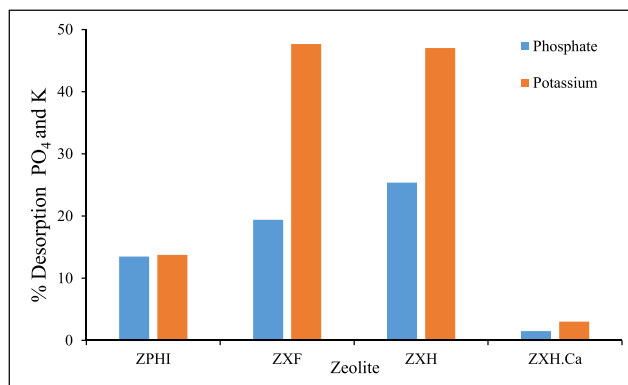


Fig. 8 Phosphate and potassium desorption from zeolites after 24 h of contact with the buffer solution (0.1 mol Na₂CO₃/ NaHCO₃)

shown in Table 9. As expected, the effluent contains significant concentrations of the nutrients of interest (44.4 mg K⁺/L and 111.4 mg PO₄³⁻/L).

Significant removal was observed for nutrients K (97%) and PO₄³⁻ (95%) after the contact with zeolite ZXH. Ca. It is expected that the adsorption process involves the binding of phosphate with Al, Ca, and Fe present in the zeolite while for potassium, it should occur by cation exchange with Na (extra framework cations). Other studies indicated in the literature using zeolites for this purpose showed removals of 50% (Dionisiou et al. 2013) and 90% of PO₄³⁻ (Yang et al. 2014) from waters enriched with P and amended sediments effluents with concentration ranging from 0 to 122 mg PO₄/L. Using technologies like graphene nanotubes, the removals were 86% (Kim et al. 2018), 85% (Tran et al. 2015), and 80% (Zou and Wang 2016), which shows the excellent performance of the zeolites tested in this work. Besides, it is crucial to note that after treatment, the concentration of phosphorus remaining in the effluent is below the emission limit. We did not find studies on potassium removal in the literature. These preliminary results suggest this zeolite as a promising adsorbent in effluent treatment. The adsorption mechanism occurs as explained in item “Phosphate and potassium adsorption in zeolite”, where phosphate ions bind to Ca, Al, and Fe ions present in zeolite, while that for potassium, cation exchange with Na ions (extra-structural cations) occurs.

It is also worth mentioning the decrease in the concentration of Na (100%) and the release of Ca (8 mg L⁻¹) and Cl

Table 7 Summary of the results of the intraparticle kinetic model application

| Sample | Film diffusion-dominated regime | | Pore diffusion-dominated regime | |
|---------|--|----------------|--|----------------|
| | Kd, f (mg-P/g zeolite-h ^{0.5}) | R ² | Kd, p (mg-P/g zeolite-h ^{0.5}) | R ² |
| ZXH | 14.48 | 1.0000 | 0.676 | 0.9952 |
| ZXF | 9.80 | 0.9229 | 1.347 | 0.9601 |
| ZPH. I | 2.88 | 0.9266 | 0.550 | 0.9194 |
| ZXH. Ca | 34.02 | 0.9825 | 5.018 | 0.9325 |

Table 8 Chemical composition of loaded and desorbed zeolites in 24-h tests with carbonate buffer and sodium bicarbonate solution

| Oxide | ZXH | | | | ZXF | | | |
|--------------------------------|-------------------|-------|-------|-------|-------------------|-------|-------|-------|
| | Content (% oxide) | | | | Content (% oxide) | | | |
| | Loaded | | | | Desorbed | | | |
| SiO ₂ | 35.37 | 39.41 | 46.22 | 37.94 | 34.37 | 44.75 | 49.60 | 32.11 |
| Al ₂ O ₃ | 27.89 | 27.20 | 31.74 | 29.45 | 26.00 | 30.04 | 32.93 | 29.25 |
| Fe ₂ O ₃ | 0.11 | 2.25 | 2.95 | 0.223 | 0.11 | 2.90 | 3.31 | 0.08 |
| K ₂ O | 11.62 | 10.35 | 9.23 | 10.97 | 6.48 | 5.98 | 2.68 | 8.05 |
| CaO | 0.48 | 1.41 | 1.95 | 11.90 | 0.39 | 1.55 | 1.72 | 12.63 |
| TiO ₂ | 0.05 | 0.58 | 0.95 | 0.05 | 0.05 | 0.76 | 1.04 | 0.04 |
| MgO | 0.14 | 0.18 | 0.54 | 0.04 | 0.18 | 0.21 | 0.57 | 0.03 |
| P ₂ O ₅ | 17.67 | 11.70 | 4.42 | 24.61 | 15.38 | 11.54 | 1.80 | 23.03 |
| Na ₂ O | 6.65 | 6.57 | 1.47 | 1.27 | 21.48 | 16.00 | 8.62 | 3.48 |
| MnO | 0.02 | 0.35 | 0.52 | 0.00 | 0.01 | 0.46 | 0.63 | 0.00 |

(396 mg L⁻¹) to the effluent. Zeolite ZXH. Ca was not washed before being used as an adsorbent, which explains the high levels of chloride in the treated effluent, coming from the process of modification of the zeolite with CaCl₂. However, the presence of chloride does not compromise its quality of the effluent, since there is no specific emission limit for this ion.

It should also be noted that preliminary tests (not shown) made with unmodified zeolite (ZXH) indicated less significant removals of K⁺ (29%) and PO₄³⁻ (77%). These results corroborate the higher adsorption capacity of modified zeolite in synthetic solutions.

Table 9 Characterization parameters of the studied effluent before and after contact with modified zeolite ZXH.Ca

| Parameter | Effluent | | | Emission limit | |
|-------------------------------|--------------------|---------------|-------------|----------------|--------|
| | Before | After contact | Removal (%) | | |
| pH | 7.30 | 9.47 | | 6.0–9.0* | |
| Conductivity | μs/cm | 381 | 391 | | |
| Na ⁺ | mg L ⁻¹ | 5.4 | < LD | 100 | |
| NH ₄ ⁺ | | 11.8 | 12 | 0 | 20 |
| K ⁺ | | 44.4 | 1.3 | 98 | |
| Mg ⁺² | | 0.6 | 0.6 | 0 | |
| Ca ⁺² | | 3.6 | 8 | 0 | |
| F ⁻ | | 1.5 | 1.4 | 7 | 10* |
| Cl ⁻ | | 126.7 | 396 | 0 | |
| SO ₄ ²⁻ | | 12.9 | 13.5 | 0 | |
| NO ₃ ⁻ | | 1.6 | 1.5 | 0.1 | |
| PO ₄ ³⁻ | | 111.4 | 6.1 | 95 | 12.3** |

Test conditions: 24 h, S/L 16, natural pH (6 ± 6.20), 200 rpm, 23 °C

*Effluent discharge limit–CONAMA resolution no. 430/2011

**Effluent discharge limit–CONSEMA resolution no. 355/2017

The desorption results carried out with the zeolite ZXH. Ca after the effluent adsorption tests (item “Desorption tests”), indicates that the release of the nutrients of interest (phosphate and potassium) was 7% for PO₄³⁻ and 100% for K⁺ of the nutrient in 24 h of analysis. It is expected that the release of nutrients occurs gradually as can be observed in the test performed with ZXH zeolites for a longer period (120 h), indicating that phosphate continues to be released. In other studies, using zeolites loaded with phosphate, the release reached 70% and 79% in 24 h of analysis (Guaya et al. 2015; Hermassi et al. 2016) using similar desorption conditions. The desorption results obtained in the present study suggest a slow phosphate release, which is more attractive for commercial applications. The higher potassium desorption (100%) is associated with the influence of the buffer solution (Na₂CO₃/NaHCO₃) through the exchange mechanism between Na and K. In fact, it was observed that sodium has been incorporated into the zeolitic material at the same time while potassium has been released. Other ions such as NH₄⁺, Ca⁺², F⁻, and NO₃⁻ were not detected, which indicates that there was no release, and SO₄²⁻ showed low concentration on solution (1.27 mg/L) suggesting a not significant release.

Conclusions

Zeolites of type X, Na-P1, and A used in this study showed different performances in terms of the adsorption capacity of PO₄ and K present in synthetic solutions and industrial effluents, with the best performance (190 mg P-PO₄/g and 346 mg K/g of zeolite) attributed to zeolite type X (ZXH), produced by the two-stage hydrothermal method (Integrated Process II). The interaction mechanism between the adsorbent and the adsorbate is due to a heterogeneous chemical interaction, which occurs in different stages and is confirmed by the

interparticular kinetic model. It was possible to observe that at acidic or very basic pHs, there is a compromise in the adsorption of nutrients due to the degradation of the zeolites or the weakening of the ion exchange, respectively. The zeolites' modification with calcium chloride resulted in an increase in the adsorption capacity of nutrients by up to four times when compared to the values reported in the literature. In the tests with the effluent, the removal capacity of the ions of interest was above 95%, which indicates the promising use of modified zeolite in nutrient recovery. The release of nutrients from modified zeolites X occurred slowly and gradually, which drives the use of the material as fertilizer.

Acknowledgments The authors are grateful to the CNPq (312489/2018-8) and Coordenação de Aperfeiçoamento de Pessoal Nível Superior – Brasil (CAPES, Código de Financiamento 001).

Availability of data and materials Data and material access are not available.

Funding Students Beatriz Bonetti and Etienne C. Waldow receive a scholarship from CNPq (312489 / 2018-8) and Coordination for the Improvement of Higher Education Personnel - Brazil (CAPES, Financing Code 001).

Compliance with ethical standards

Ethics approval and consent to participate Not applicable

Competing interests The authors declare that they have no competing interests.

Consent for publication Not applicable

References

- Abruzzi RC (2017) Aplicação de nanopartículas de SnO₂ e zeólitas em Porto Alegre Março, 2017 Porto Alegre Março, 2017. Pontifícia Universidade Católica do Rio Grande do Sul
- Aquino TF (2018) Síntese de zeólitas do tipo X a partir de cinzas volantes e de fundo de carvão mineral para a captura de CO₂. Universidade Federal De Santa Catarina
- Bergaut V, Singer A (1996) High capacity cation exchanger by hydrothermal zeolitization of coal fly ash. *Appl Clay Sci* 10:369–378. [https://doi.org/10.1016/0169-1317\(95\)00033-X](https://doi.org/10.1016/0169-1317(95)00033-X)
- Bernardi ACDC (2008) Potencial do uso de zeólitas na agropecuária. *Embrapa Pecuária Sudeste* 46. <https://doi.org/10.1016/S0194>
- Bhardwaj D, Sharma P, Sharma M, Tomar R (2014) Removal and slow release studies of phosphate on surfactant loaded hydrothermally synthesized silicate nanoparticles. *J Taiwan Inst Chem Eng* 45: 2649–2658. <https://doi.org/10.1016/j.jtice.2014.07.010>
- Brassell JP, Ojumu TV, Petrik LF (2016) Upscaling of zeolite synthesis from coal fly ash waste: current status and future outlook. In: *Zeolites - useful minerals*
- Bruulsema T (2018) Managing nutrients to mitigate soil pollution. *Environ Pollut* 243:1602–1605. <https://doi.org/10.1016/j.envpol.2018.09.132>
- Canpolat F, Yilmaz K, Köse MM et al (2004) Use of zeolite, coal bottom ash and fly ash as replacement materials in cement production. *Cem Concr Res* 34:731–735. [https://doi.org/10.1016/S0008-8846\(03\)00063-2](https://doi.org/10.1016/S0008-8846(03)00063-2)
- Cardoso AM, Horn MB, Ferret LS, Azevedo CMN, Pires M (2015a) Integrated synthesis of zeolites 4A and Na-P1 using coal fly ash for application in the formulation of detergents and swine wastewater treatment. *J Hazard Mater* 287:69–77
- Cardoso AM, Paprocki A, Ferret LS, Azevedo CMN, Pires M (2015b) Synthesis of zeolite Na-P1 under mild conditions using Brazilian coal fly ash and its application in wastewater treatment. *Fuel* 139: 59–67. <https://doi.org/10.1016/j.fuel.2014.08.016>
- Cheng Q, Li H, Xu Y, Chen S, Liao Y, Deng F, Li J (2017) Study on the adsorption of nitrogen and phosphorus from biogas slurry by NaCl-modified zeolite. *PLoS One* 12:1–12. <https://doi.org/10.1371/journal.pone.0176109>
- Chmielewska E, Hodossyová R, Bujdoš M (2013) Kinetic and thermodynamic studies for phosphate removal using natural adsorption materials. *Pol J Environ Stud* 22:1307–1316
- Choi J, Chung J, Lee W, Kim JO (2016) Phosphorous adsorption on synthesized magnetite in wastewater. *J Ind Eng Chem* 34:198–203. <https://doi.org/10.1016/j.jiec.2015.11.008>
- Collins F, Rozhkovskaya A, Outram JG, Millar GJ (2020) A critical review of waste resources, synthesis, and applications for Zeolite LTA. *Microporous Mesoporous Mater* 291:109667. <https://doi.org/10.1016/j.micromeso.2019.109667>
- Dionisiou NS, Matsi T, Misopolinos ND (2013) Phosphorus adsorption-desorption on a surfactant-modified natural zeolite: A laboratory study. *Water Air Soil Pollut* 224. <https://doi.org/10.1007/s11270-012-1362-7>
- Ehsan A, Bhatti HN, Iqbal M, Noreen S (2017) Native, acidic pre-treated and composite clay efficiency for the adsorption of dicationic dye in aqueous medium. *Water Sci Technol* 75:753–764
- Fan Y, Li Y, Wu D, Li C, Kong H (2017) Application of zeolite/hydrous zirconia composite as a novel sediment capping material to immobilize phosphorus. *Water Res* 123. <https://doi.org/10.1016/j.watres.2017.06.031>
- Ferrarini SFSF, Cardoso AMAMAM, Paprocki A, Pires M (2016) Integrated synthesis of zeolites using coal fly ash: Element distribution in the products, washing waters and effluent. *J Braz Chem Soc* 27:2034–2045. <https://doi.org/10.5935/0103-5053.20160093>
- Flores CG, Schneider H, Marcilio NR, Ferret L, Oliveira JCP (2017) Potassic zeolites from Brazilian coal ash for use as a fertilizer in agriculture. *Waste Manag* 70:263–271. <https://doi.org/10.1016/j.wasman.2017.08.039>
- Gollakota ARK, Volli V, Shu CM (2019) Progressive utilisation prospects of coal fly ash: a review. *Sci Total Environ* 672:951–989
- Goscianska J, Ptaszkowska-Koniarska M, Frankowski M, Franus M, Panek R, Franus W (2018) Removal of phosphate from water by lanthanum-modified zeolites obtained from fly ash. *J Colloid Interface Sci* 513:72–81. <https://doi.org/10.1016/j.jcis.2017.11.003>
- Guaya D, Valderrama C, Farran A, Armijos C, Cortina JL (2015) Simultaneous phosphate and ammonium removal from aqueous solution by a hydrated aluminum oxide modified natural zeolite. *Chem Eng J* 271:204–213. <https://doi.org/10.1016/j.cej.2015.03.003>
- Guaya D, Valderrama C, Farran A, Cortina JL (2016) Modification of a natural zeolite with Fe (III) for simultaneous phosphate and ammonium removal from aqueous solutions. *J Chem Technol Biotechnol* 91:1737–1746. <https://doi.org/10.1002/jctb.4763>
- Guo H, White JC, Wang Z, Xing B (2018) Nano-enabled fertilizers to control the release and use efficiency of nutrients. *Curr Opin Environ Sci Health* 6:77–83. <https://doi.org/10.1016/j.coesh.2018.07.009>
- Hamdi N, Srasra E (2012) Removal of phosphate ions from aqueous solution using Tunisian clays minerals and synthetic zeolite. *J Environ Sci* 24:617–623. [https://doi.org/10.1016/S1001-0742\(11\)60791-2](https://doi.org/10.1016/S1001-0742(11)60791-2)

- Harikishore Kumar Reddy D, Vijayaraghavan K, Kim JA, Yun YS (2017) Valorisation of post-sorption materials: Opportunities, strategies, and challenges. *Adv Colloid Interf Sci* 242:35–58. <https://doi.org/10.1016/j.cis.2016.12.002>
- He Y, Lin H, Dong Y, Liu Q, Wang L (2016) Simultaneous removal of ammonium and phosphate by alkaline-activated and lanthanum-impregnated zeolite. *Chemosphere* 164:387–395. <https://doi.org/10.1016/j.chemosphere.2016.08.110>
- He Y, Lin H, Dong Y, Wang L (2017) Preferable adsorption of phosphate using lanthanum-incorporated porous zeolite: Characteristics and mechanism. *Appl Surf Sci* 426:995–1004. <https://doi.org/10.1016/j.apsusc.2017.07.272>
- Hemalatha T, Ramaswamy A (2017) A review on fly ash characteristics – Towards promoting high volume utilization in developing sustainable concrete. *J Clean Prod* 147:546–559
- Hermassi M, Valderrama C, Moreno N, Font O, Querol X, Batis N, Cortina JL (2016) Powdered Ca-activated zeolite for phosphate removal from treated waste-water. *J Chem Technol Biotechnol* 91:1962–1971. <https://doi.org/10.1002/jctb.4867>
- Hu T, Gao W, Liu X et al (2017) Synthesis of zeolites Na-A and Na-X from tablet compressed and calcinated coal fly ash. *R Soc Open Sci* 4. <https://doi.org/10.1098/rsos.170921>
- Iqbal A, Sattar H, Haider R, Munir S (2019) Synthesis and characterization of pure phase zeolite 4A from coal fly ash. *J Clean Prod* 219:258–267. <https://doi.org/10.1016/j.jclepro.2019.02.066>
- Izidoro J d C (2013) Cinzas volantes do carvão. USP
- Jha B, Singh DN (2016) Fly Ash Zeolites. *Adv Struct Mater*. <https://doi.org/10.1007/978-981-10-1404-8>
- Ji X, Zhang M, Wang Y, Song Y, Ke Y, Wang Y (2015) Immobilization of ammonium and phosphate in aqueous solution by zeolites synthesized from fly ashes with different compositions. *J Ind Eng Chem* 22:1–7. <https://doi.org/10.1016/j.jiec.2014.06.017>
- Jiang C, Jia L, He Y, Zhang B, Kirumba G, Xie J (2013) Adsorptive removal of phosphorus from aqueous solution using sponge iron and zeolite. *J Colloid Interface Sci* 402:246–252. <https://doi.org/10.1016/j.jcis.2013.03.057>
- Juan R, Hernández S, Andrés JM, Ruiz C (2007) Synthesis of granular zeolitic materials with high cation exchange capacity from agglomerated coal fly ash. *Fuel* 86:1811–1821. <https://doi.org/10.1016/j.fuel.2007.01.011>
- Kanwal A, Bhatti HN, Iqbal M, et al (2017) Basic dye adsorption onto clay/MnFe 2 O 4 composite : a mechanistic study. 2. <https://doi.org/10.2175/106143017X14839994522984>
- Kausar A, Iqbal M, Javed A, Aftab K, Nazli ZIH, Bhatti HN, Nouren S (2018) Dyes adsorption using clay and modified clay: a review. *J Mol Liq* 256:395–407. <https://doi.org/10.1016/j.molliq.2018.02.034>
- Kim JH, Kim SB, Lee SH, Choi JW (2018) Laboratory and pilot-scale field experiments for application of iron oxide nanoparticle-loaded chitosan composites to phosphate removal from natural water. *Environ Technol (UK)* 39:770–779. <https://doi.org/10.1080/09593330.2017.1310937>
- Lateef A, Nazir R, Jamil N, Alam S, Shah R, Khan MN, Saleem M (2016) Synthesis and characterization of zeolite based nano-composite: an environment friendly slow release fertilizer. *Microporous Mesoporous Mater* 232:174–183. <https://doi.org/10.1016/j.micromeso.2016.06.020>
- Liu C, Ma H, Gao Y (2019) Hydrothermal processing on potassic syenite powder: zeolite synthesis and potassium release kinetics. *Adv Powder Technol* 30:2483–2491. <https://doi.org/10.1016/j.apt.2019.07.024>
- Lopes TR (2017) Utilização de RMN no estado sólido em uma abordagem multinuclear para estudo de materiais carbonosos porosos Utilização de RMN no estado sólido em uma abordagem multinuclear para estudo de materiais carbonosos porosos. UNIVERSIDADE FEDERAL DO ESPÍRITO SANTO
- Manto MJ, Xie P, Keller MA, Liano WE, Pu T, Wang C (2017) Recovery of inorganic phosphorus using copper-substituted ZSM-5. *ACS Sustain Chem Eng* 5:6192–6200. <https://doi.org/10.1021/acssuschemeng.7b01127>
- Melo CR, Riella HG (2010) Síntese de zeólita tipo NaA a partir de caulim para obtenção de zeólita 5A através de troca iônica. *Cerâmica* 56:340–346. <https://doi.org/10.1590/s0366-69132010000400005>
- Mitrogiannis D, Psychoyou M, Baziotis I, Inglezakis VJ, Koukouzas N, Tsoukalas N, Palles D, Kamitsos E, Oikonomou G, Markou G (2017) Removal of phosphate from aqueous solutions by adsorption onto Ca (OH)₂treated natural clinoptilolite. *Chem Eng J* 320:510–522. <https://doi.org/10.1016/j.cej.2017.03.063>
- Nausheen S, Bhatti HN, Hanif MA (2017) Enhanced removal of golden XGL dye by clay composites : batch and column studies. *Pol J Environ Stud* 26:2113–2123. <https://doi.org/10.15244/pjoes/68535>
- Onyango MS, Kuchar D, Kubota M, Matsuda H (2007) Adsorptive removal of phosphate ions from aqueous solution using synthetic zeolite. *Ind Eng Chem Res* 46:894–900. <https://doi.org/10.1021/ie060742m>
- Pearce HA (1975) Zeolite molecular sieves—Structure, chemistry and use. *J Chromatogr A* 106:499. [https://doi.org/10.1016/s0021-9673\(00\)93871-8](https://doi.org/10.1016/s0021-9673(00)93871-8)
- Pengthamkeerati P, Satapanajaru T, Chularuengsookorn P (2008) Chemical modification of coal fly ash for the removal of phosphate from aqueous solution. *Fuel* 87:2469–2476. <https://doi.org/10.1016/j.fuel.2008.03.013>
- Petrov I, Michalev T (2012) Synthesis of Zeolite A: A Review. НАУЧНИ ТРУДОВЕ НА РУСЕНСКИЯ УНИВЕРСИТЕТ. *Proc Chem Technol* 30–35
- Philippi M, dos Santos HS, Martins AO, Azevedo CMN, Pires M (2007) Alternative spectrophotometric method for standardization of chlorite aqueous solutions. *Anal Chim Acta* 585:361–365. <https://doi.org/10.1016/j.aca.2006.12.053>
- Querol X, Moreno N, Umaa JC et al (2002) Synthesis of zeolites from coal fly ash: an overview. *Int J Coal Geol* 50:413–423. [https://doi.org/10.1016/S0166-5162\(02\)00124-6](https://doi.org/10.1016/S0166-5162(02)00124-6)
- Reddy DHK, Vijayaraghavan K, Kim JA, Yun YS (2017) Valorisation of post-sorption materials: opportunities, strategies, and challenges. *Adv Colloid Interface Sci* 242. <https://doi.org/10.1016/j.cis.2016.12.002>
- Rhodes CJ (2010) Properties and applications of zeolites. *Sci Prog* 93:223–284. <https://doi.org/10.3184/003685010X12800828155007>
- da Rocha Junior PR, Andrade FV, Mendonça E d S et al (2017) Soil, water, and nutrient losses from management alternatives for degraded pasture in Brazilian Atlantic Rainforest biome. *Sci Total Environ* 583:53–63. <https://doi.org/10.1016/j.scitotenv.2016.12.187>
- Sandomierski M, Buchwald Z, Koczorowski W, Voelkel A (2019) Calcium forms of zeolites A and X as fillers in dental restorative materials with remineralizing potential. *Microporous Mesoporous Mater* 294:109899. <https://doi.org/10.1016/j.micromeso.2019.109899>
- Sharma P, Song JS, Han MH, Cho CH (2016) GIS-NaP1 zeolite microspheres as potential water adsorption material: Influence of initial silica concentration on adsorptive and physical/topological properties. *Sci Rep* 6:1–26. <https://doi.org/10.1038/srep22734>
- Shi J, Yang Z, Dai H, Lu X, Peng L, Tan X, Shi L, Fahim R (2017) Preparation and application of modified zeolites as adsorbents in wastewater treatment. *Water Sci Technol* 2017:621–635. <https://doi.org/10.2166/wst.2018.249>
- Tran DNH, Kabiri S, Wang L, Losic D (2015) Engineered graphene-nanoparticle aerogel composites for efficient removal of phosphate from water. *J Mater Chem A* 3:6844–6852. <https://doi.org/10.1039/c4ta06308b>
- Van Raj B (2011) Melhorando o ambiente radicular em subsuperfície. *Int Plant Nutr Inst*

- Vilar CC, Costa ACS, Hoepers A, Junior IGS (2010) Capacidade máxima de adsorção de fósforo relacionada a formas de ferro e alumínio em solos subtropicais. *R Bras Ci Solo* 34:1059–1068
- Wan C, Ding S, Zhang C, Tan X, Zou W, Liu X, Yang X (2017) Simultaneous recovery of nitrogen and phosphorus from sludge fermentation liquid by zeolite adsorption: Mechanism and application. *Sep Purif Technol* 180:1–12. <https://doi.org/10.1016/j.seppur.2017.02.031>
- Wang S, Peng Y (2010) Natural zeolites as effective adsorbents in water and wastewater treatment. *Chem Eng J*
- Wu D, Sui Y, Chen X, He S, Wang X, Kong H (2008) Changes of mineralogical-chemical composition, cation exchange capacity, and phosphate immobilization capacity during the hydrothermal conversion process of coal fly ash into zeolite. *Fuel* 87:2194–2200. <https://doi.org/10.1016/j.fuel.2007.10.028>
- Xie J, Wang Z, Fang D, Li C, Wu D (2014) Green synthesis of a novel hybrid sorbent of zeolite/lanthanum hydroxide and its application in the removal and recovery of phosphate from water. *J Colloid Interface Sci* 423:13–19. <https://doi.org/10.1016/j.jcis.2014.02.020>
- Yang L, Qian X, Yuan P, Bai H, Miki T, Men F, Li H, Nagasaka T (2019) Green synthesis of zeolite 4A using fly ash fused with synergism of NaOH and Na₂CO₃. *J Clean Prod* 212:250–260. <https://doi.org/10.1016/j.jclepro.2018.11.259>
- Yang M, Lin J, Zhan Y, Zhang H (2014) Adsorption of phosphate from water on lake sediments amended with zirconium-modified zeolites in batch mode. *Ecol Eng* 71:223–233. <https://doi.org/10.1016/j.ecoleng.2014.07.035>
- Yoldi M, Fuentes-Ordoñez EG, Korili SA, Gil A (2019) Zeolite synthesis from industrial wastes. *Microporous Mesoporous Mater* 287:183–191. <https://doi.org/10.1016/j.micromeso.2019.06.009>
- Zhan Y, Zhang H, Lin J, Zhang Z, Gao J (2017) Role of zeolite's exchangeable cations in phosphate adsorption onto zirconium-modified zeolite Yanhui. *J Mol Liq* 243:624–637. <https://doi.org/10.1016/j.molliq.2017.08.091>
- Zhang M, Gao B, Yao Y, Xue Y, Inyang M (2012) Synthesis of porous MgO-biochar nanocomposites for removal of phosphate and nitrate from aqueous solutions. *Chem Eng J* 210:26–32. <https://doi.org/10.1016/j.cej.2012.08.052>
- Zou H, Wang Y (2016) Phosphorus removal and recovery from domestic wastewater in a novel process of enhanced biological phosphorus removal coupled with crystallization. *Bioresour Technol* 211:87–92. <https://doi.org/10.1016/j.biortech.2016.03.073>

Publisher's note Springer Nature remains neutral with regard to jurisdictional claims in published maps and institutional affiliations.